





RESEARCH ARTICLE | JULY 24 2024

Diffusion-driven instabilities in the BT-GN oscillatory carbonylation reaction network

Stevan Maćešić   ; Katarina Novakovic  



Chaos 34, 073152 (2024)

<https://doi.org/10.1063/5.0211536>



AIP Advances

Why Publish With Us?

-  **25 DAYS**
average time to 1st decision
-  **740+ DOWNLOADS**
average per article
-  **INCLUSIVE**
scope

[Learn More](#)



Diffusion-driven instabilities in the BT-GN oscillatory carbonylation reaction network

Cite as: Chaos 34, 073152 (2024); doi: 10.1063/5.0211536

Submitted: 31 March 2024 · Accepted: 1 July 2024 ·

Published Online: 24 July 2024



View Online



Export Citation



CrossMark

Stevan Maćešić^{1,a)}  and Katarina Novakovic^{2,a)} 

AFFILIATIONS

¹Faculty of Physical Chemistry, University of Belgrade, Studentski trg 12-16, Belgrade, Serbia

²School of Engineering, Newcastle University, Newcastle upon Tyne NE1 7RU, United Kingdom

^{a)}Authors to whom correspondence should be addressed: stevan.macesic@ffh.bg.ac.rs and katarina.novakovic@newcastle.ac.uk

ABSTRACT

This study explores the role of diffusion in creating instabilities in the Bruk Temkin-Gorodsky Novakovic (BT-GN) oscillatory carbonylation reaction network. Stoichiometric network analysis and numerical methods revealed the presence of two destabilizing feedback cycles responsible for these instabilities. Analysis of a spatially uniform system showed that the saddle-node bifurcation can be simulated within the reaction network. The introduction of diffusion results in two types of instabilities: one occurs when a spatially uniform system is already unstable, leading to a reaction-diffusion front; and another involves diffusion-driven instabilities where introducing diffusion destabilizes a stable spatially uniform system. Slower PdI₂ diffusion plays a key role in inducing these instabilities. Equations describing conditions for the emergence of the instabilities in both cases were derived.

© 2024 Author(s). All article content, except where otherwise noted, is licensed under a Creative Commons Attribution (CC BY) license (<https://creativecommons.org/licenses/by/4.0/>). <https://doi.org/10.1063/5.0211536>

This study investigates the emergence of oscillatory dynamics in a Bruk Temkin-Gorodsky Novakovic (BT-GN) oscillatory carbonylation reaction network, employing a combination of stoichiometric network analysis and numerical simulations. The study examines the interplay between reaction kinetics and diffusion, identifying key feedback loops that drive instability in this system. Notably, the introduction of diffusion was found to yield two distinct types of instabilities: reaction-diffusion fronts and Turing patterns. The latter, arising from a stable system destabilized by diffusion, highlights the crucial role of spatial heterogeneity in pattern formation. This research provides valuable insights into the complex dynamics of reaction-diffusion systems, with implications for diverse fields ranging from material science to biological pattern formation.

I. INTRODUCTION

Pattern formation in nature (e.g., stripes in zebras and spots in leopards) was a subject of Alan Turing theory of the chemical basis of morphogenesis, where the feasibility of homogeneous uniform state to progress to pattern formation was proposed to take place via instability resulting from the interaction of chemical reaction

and the difference in diffusion coefficients of the chemical species involved.^{1,2} The appearance of Turing patterns is vast and includes fronts, hexagons, spirals, stripes, and dissipative solutions observed and linked with a broad range of phenomena in biological systems and beyond.³⁻¹⁵ When chemical reactions are examined under laboratory conditions, systems that produce Turing patterns are scarce and commonly linked to oscillatory chemical reactions in which two or more chemical species are oscillating. Experimentally, the patterns are captured in the Belousov Zhabotinsky reaction, as well as the Briggs-Rauscher and Chlorite-Iodide-Malonic Acid (CIMA) reactions,¹⁶⁻²⁴ with real-life applications of such observations yet to materialize. Looking for further examples of the existence of Turing patterns in oscillatory reaction systems that potentially can lead to new discoveries and applications, the study reported here focuses on the Bruk Temkin-Gorodsky Novakovic (BT-GN) reaction, an oscillatory carbonylation reaction employing poly(ethylene glycol) methyl ether acetylene (PEGA) as a substrate.²⁵ This oscillatory chemical reaction is unusual and stands out from other oscillatory chemical reactions. It is an organic chemical oscillator, where complex products are formed from simple starting materials.²⁶⁻²⁸ In addition to oscillations in pH and redox potential, it can produce oscillations in turbidity, and heat is released from the reaction in a pulsed stepwise manner.²⁹⁻³² Importantly, progress in experimental

studies of this chemical system led to the portfolio of substrates which, in addition to small molecule substrates such as phenylacetylene, now include polymeric substrates based on PEGylated alkynes.^{25,33} Equally, it has been demonstrated experimentally that in addition to small molecule catalysts [e.g., palladium(II) iodide], oscillatory carbonylation reactions are also feasible when polymeric catalysts are used (e.g., imine functionalized chitosan-palladium).³⁴ Transition to polymeric substrates and catalysts allowed the opening of a new chapter in the studies of oscillatory carbonylation processes and led to the proof-of-concept development of oscillatory (pulsatile) materials intended for pulsatile drug release and other useful applications.³⁵ The study reported here employs a mathematical modeling approach to explore the BT-GN reaction system to determine feasibility and conditions that could yield Turing patterns.

In order to effectively evaluate and control the behavior of temporal and spatiotemporal phenomena, it is crucial to have a comprehensive understanding of the conditions under which they can occur. A key factor in achieving this goal is an accurate mathematical model based on a realistic chemical network. As part of the modeling process, performing linear stability analysis plays an essential role, as it ensures that the proposed model generates correct dynamics. Linear stability analysis of the reaction–diffusion system is based on solving analytically the steady-state problem and then evaluating eigenvalues of the Jacobian to determine stability and the type of bifurcations.³⁶ Realistic chemical networks usually have more than three intermediate species (variables), while analytical solutions can usually only be found in the case of a max of three variables. Therefore, analysis of the reaction–diffusion system encountered in chemistry was usually done on the networks with two or three intermediate species while in the case of the reaction networks with more species, analysis was usually limited to numerical investigation. To overcome this problem in our previous work,³⁷ a method based on stoichiometric network analysis (SNA)^{38,39} was presented. In this approach, analysis can be done efficiently on very complex chemical networks incorporating more than three intermediate species. Furthermore, the analytical form of instability conditions for the emergence of diffusion-driven instabilities, which can be used to optimize experimental conditions, can be efficiently derived. This approach also facilitates the detection of important processes and intermediate species involved in the emergence of diffusion-driven instabilities. Hence, taking into account all

advantages, this approach was used to analyze the BT-GN reaction system.

The study reported here commences with a basic reaction network of the BT-GN reaction system, substantiated with the experimental evidence²⁵ and proceeds to examine two sets of conditions: one for a well-stirred reactor (a spatially uniform system) and another where diffusion is present (a spatially nonuniform system). The aim was to gain a comprehensive understanding of the stability boundaries in this system under different conditions. The study also focuses on determining the conditions for diffusion-driven instabilities. This study also aims to build on our previous work³⁷ related to the reaction–diffusion systems and expand our understanding of how conservation constraints affect the steady-state stability of the reaction networks in the presence of diffusion.

II. MODEL

The reaction network of the oscillatory carbonylation reaction employing poly(ethylene glycol) methyl ether acetylene (PEGA) as a substrate and palladium iodide (PdI₂) as a catalyst used in this study is given in Table I.

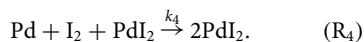
The proposed reaction network simulates the dynamics of a system comprising PEGA as substrate, PdI₂/KI as catalyst, and methanol as both reactant and solvent. The system is purged with CO and air in a semi-batch configuration, which is known to produce several hours of oscillatory dynamics under certain initial conditions.²⁵ This reaction network describes the process of oscillatory carbonylation through a series of six chemical reactions, where reaction rates (R_5) and (R_{-5}) come from a direct and reversible reaction in equilibrium. The model includes 11 chemical species: PEGA, PdI₂, HI, CH₃OH, CO, PEGP, Pd, O₂, I₂, H₂O, and IPdR (where R stands for COOCH₃). Among these species, PEGA, CH₃OH, O₂, and CO are reactants, while PEGP represents the main diester product of the reaction (poly(ethylene glycol)methyl ether (Z)-5-methoxy-3-(methoxycarbonyl)-5-oxopent-3-enoate).³¹ PdI₂, HI, Pd, I₂, and IPdR serve as intermediate species and play a crucial role in determining the system's dynamics. Although PdI₂ is added to the system to initiate the reaction, it is considered an intermediate species. Alternatively, if treated as an external species with constant concentration, it would disrupt the feedback cycles required for the proper functioning of the reaction network considered. Due to an excess of CH₃OH and purging by

TABLE I. A set of reactions representing the model studied.²⁵ Note: R stands for COOCH₃.

Reactions	Reaction rates
$PEGA + PdI_2 + 2HI + 2CH_3OH + 2CO \xrightarrow{k_1} PEGP + Pd + 4 HI$	$r_1 = k_1 [PEGA]_0 [PdI_2] [HI]^2 \quad (R_1)$
$2HI + 0.5 O_2 \xrightarrow{k_2} I_2 + H_2O$	$r_2 = k_2 [HI]^2 \quad (R_2)$
$Pd + I_2 \xrightarrow{k_3} PdI_2$	$r_3 = k_3 [Pd] [I_2] \quad (R_3)$
$Pd + I_2 \xrightarrow{k_4} PdI_2$	$r_4 = k_4 [Pd] [I_2] [PdI_2] \quad (R_4)$
$PdI_2 + CH_3OH + CO \xrightleftharpoons[k_{-5}]{k_5} IPdR + HI$	$r_5 = k_5 [PdI_2] \quad (R_5)$
	$r_{-5} = k_{-5} [IPdR] [HI] \quad (R_{-5})$

O₂ and CO, their concentrations were considered constant.^{28,40–43} They were not included in the reaction rates associated with the proposed reaction network but were incorporated into the corresponding rate constants. PEGA is consumed only by reaction (R₁), causing its concentration to decrease over time. However, this occurs much more slowly than other reactions in the overall process. Therefore, the PEGA concentration is considered to be constant, assuming that the system is in a pseudo-steady-state. This constant PEGA concentration was used for stability analysis and numerical simulations.

In the reaction network presented in Table I,²⁵ reactions (R₁) and (R₄) are postulated to be autocatalytic. Reaction (R₁) is assumed to be autocatalytic in hydrogen iodide species, which is considered to be the source of oscillations in hydrogen ions and, therefore, pH oscillations in this system. However, (R₄) was postulated to represent the autocatalysis of PdI₂, but the stoichiometry of reaction (R₄) does not align with the expression of reaction rates based on mass action kinetics. The adjustments were made to rectify this discrepancy without altering the structure of the reaction network.⁴⁴ The revised expression for the reaction (R₄) is provided below and is subsequently used in place of Reaction 4 given in Table 1.



In our simulations, mass action kinetics was used to describe the kinetics of chemical reactions in both spatially uniform and nonuniform systems. In the case of a spatially uniform system, the temporal dynamics of the concentrations of the intermediate species PdI₂, HI, Pd, I₂, and IPdR is described by the following set of ordinary differential equations (ODEs),

$$\begin{aligned} \frac{d[\text{PdI}_2]}{dt} &= -r_1 + r_3 + r_4 - r_5 + r_{-5}, \\ \frac{d[\text{HI}]}{dt} &= 2r_1 - 2r_2 + r_5 - r_{-5}, \\ \frac{d[\text{Pd}]}{dt} &= r_1 - r_3 - r_4, \\ \frac{d[\text{I}_2]}{dt} &= r_2 - r_3 - r_4, \\ \frac{d[\text{IPdR}]}{dt} &= r_5 - r_{-5}, \end{aligned} \quad (1)$$

where the expressions for the reaction rates r_i are defined in Table I. In the case of a spatially nonuniform system, the following set of reaction–diffusion equations was used:

$$\begin{aligned} \frac{d[\text{PdI}_2]}{dt} &= D_1 \nabla^2 [\text{PdI}_2] - r_1 + r_3 + r_4 - r_5 + r_{-5}, \\ \frac{d[\text{HI}]}{dt} &= D_2 \nabla^2 [\text{HI}] + 2r_1 - 2r_2 + r_5 - r_{-5}, \\ \frac{d[\text{Pd}]}{dt} &= D_3 \nabla^2 [\text{Pd}] + r_1 - r_3 - r_4, \end{aligned} \quad (2)$$

$$\begin{aligned} \frac{d[\text{I}_2]}{dt} &= D_4 \nabla^2 [\text{I}_2] + r_2 - r_3 - r_4, \\ \frac{d[\text{IPdR}]}{dt} &= D_5 \nabla^2 [\text{IPdR}] + r_5 - r_{-5}, \end{aligned}$$

where ∇^2 represents the Laplacian operator while D_1 – D_5 are the diffusion coefficient of intermediate species PdI₂, HI, Pd, I₂, and IPdR, respectively.

III. METHODS

A. Numerical simulations

Numerical methods were used to solve ODEs and partial differential equations (PDEs) representing dynamics of the PEGA reaction network under spatially uniform and nonuniform conditions. To solve ODEs describing the PEGA reaction network dynamics under a spatially uniform system, a MATLAB `odes15s` function was used. To solve PDEs representing dynamics of the system under spatially nonuniform conditions, FENICS package⁴⁵ was used. FENICS package employs a finite element method to solve PDEs. An implicit Euler scheme was used to discretize time in the PDEs.

To effectively simulate the thin layer of solution in a reaction–diffusion system, a circular computational domain with a radius of 5 cm was used. Homogeneous Neumann boundary conditions⁴⁶ were applied at the boundaries. Initially, a uniform distribution of concentrations for intermediate species PdI₂, HI, Pd, I₂, and IPdR was considered within this domain to maintain simplicity for the initial conditions of the reaction network model. The only exception to this uniform distribution was at the center—a smaller circular area with a radius of 0.005 cm where concentrations were set at double relative to the rest of the domain to model localized variations in concentration that may occur in practical scenarios like the addition of reactants at specific locations within the reactor.

B. Stoichiometric network analysis

Linear stability analysis in SNA^{37–39,47,48} is based on finding a positive solution of the steady-state equation^{38,47,49,50}

$$\mathbf{S} \mathbf{r}_{ss} = 0, \quad (3)$$

where \mathbf{S} is the stoichiometric matrix related to intermediate species of considered reaction network while \mathbf{r}_{ss} is the vector of reaction rates at the steady state. In matrix \mathbf{S} , each row corresponds to an intermediate species and each column corresponds to a reaction defined in the model. Therefore, element S_{ij} is defined as the difference between the stoichiometric coefficients of intermediate species c_i on the right and left side of the reaction R_j ($S_{ij} = S_{ij}^R - S_{ij}^L$). Positive solutions of Eq. (1) are found in the form of the matrix of extreme currents \mathbf{E} . Having matrix \mathbf{E} calculated, vector \mathbf{r}_{ss} can be represented as a positive linear combination using the relation^{38,39}

$$\mathbf{r}_{ss} = \mathbf{E} \mathbf{j}, \quad (4)$$

where vector \mathbf{j} represents current rates, with each rate j_i indicating the contributions of corresponding extreme current E_i (a column of matrix \mathbf{E}). The use of matrix \mathbf{E} and Eq. (4) allows for the decomposition of the entire network into steady-state subnetworks, making it easy to evaluate their impact on stability.

For steady-state stability evaluation, the calculation of Jacobian is essential. For spatially uniform systems, the Jacobian is defined as^{38,39}

$$\mathbf{M}(\mathbf{j}, \mathbf{h}) = -\mathbf{V}(\mathbf{j})\text{diag}(\mathbf{h}), \quad (5)$$

where \mathbf{h} is a vector of reciprocal steady-state concentrations of intermediate species, while $\mathbf{V}(\mathbf{j})$ is a *current rate matrix* defined as³⁸

$$\mathbf{V}(\mathbf{j}) = -\text{Sdiag}(\mathbf{E}\mathbf{j})\mathbf{K}^T, \quad (6)$$

where \mathbf{K} is the matrix of the order of reactions, while T stands for matrix transpose. Similarly to matrix \mathbf{S} , in matrix \mathbf{K} , each row corresponds to one of the intermediate species and each column corresponds to one of the reactions defined in the model. In this case, element $K_{i,j}$ represents the stoichiometric coefficient of intermediate species c_i on the left side of a chemical reaction ($K_{i,j} = S_{i,j}^L$). For spatially nonuniform systems, Jacobian \mathbf{M}_{RD} is divided into two parts: one corresponding to the Jacobian of spatially uniform system \mathbf{M} defined in Eq. (5) and also includes the diffusion part. Matrix \mathbf{M}_{RD} is defined as^{38,51}

$$\mathbf{M}_{\text{RD}} = \mathbf{M} - \omega^2\text{diag}(\mathbf{D}), \quad (7)$$

where ω is the real number that determines the spatial frequency of perturbations also known as wave vector.^{16,36,38,51} This term emerges as a result of the linearization of the system around steady-state where Fourier transformation is applied in order to handle spatial terms in Eq. (2).

Steady-state stability in SNA is evaluated using Hurwitz determinants Δ_i or α approximation criteria.^{38,52,53} These are used to assess spatially uniform and nonuniform systems for steady-state stability. For saddle-node (SN) bifurcation to occur, it requires that $\alpha_n = 0$, while Andronov-Hopf (AH) bifurcation occurs when $\Delta_{n-i} = 0$ (index n corresponds to the number of intermediate species—variables in the system).⁵⁴ The α approximation is typically utilized for large chemical systems where at least one coefficient of characteristic polynomial $\alpha_1 - \alpha_n$ needs to be negative for an unstable steady state to occur. Conditions for AH emergence are derived from $\alpha_1 - \alpha_{n-1}$, while the condition for SN remains unchanged. In spatially uniform systems, steady-state stability can also be determined by analyzing the diagonal minors of $\mathbf{V}(\mathbf{j})$, indicating instability if a negative diagonal minor exists. Despite being an approximation, this approach generally yields reliable results.^{37,48,55-58}

IV. RESULTS AND DISCUSSION

A. Stability analysis of a spatially uniform system

The first step in the analysis involves creating the \mathbf{S} and \mathbf{K} matrices which are, for the model under consideration, defined by Eqs. (8) and (9), respectively,

$$\mathbf{S} = \begin{bmatrix} -1 & 0 & 1 & 1 & -1 & 1 \\ 2 & -2 & 0 & 0 & 1 & -1 \\ 1 & 0 & -1 & -1 & 0 & 0 \\ 0 & 1 & -1 & -1 & 0 & 0 \\ 0 & 0 & 0 & 0 & 1 & -1 \end{bmatrix} \begin{matrix} \text{PdI}_2 \\ \text{HI} \\ \text{Pd} \\ \text{I}_2 \\ \text{IPdR} \end{matrix}, \quad (8)$$

$$\mathbf{K} = \begin{bmatrix} 1 & 0 & 0 & 1 & 1 & 0 \\ 2 & 2 & 0 & 0 & 0 & 1 \\ 0 & 0 & 1 & 1 & 0 & 0 \\ 0 & 0 & 1 & 1 & 0 & 0 \\ 0 & 0 & 0 & 0 & 0 & 1 \end{bmatrix} \begin{matrix} \text{PdI}_2 \\ \text{HI} \\ \text{Pd} \\ \text{I}_2 \\ \text{IPdR} \end{matrix}. \quad (9)$$

Upon analysis of matrix \mathbf{S} , it was determined that its rank is 3 while there are five intermediate species. As a result, two conservation constraints can be derived from this analysis, which are presented in the form of the conservation matrix \mathbf{C} [Eq. (10), further information available in Appendix III in the supplementary material],

$$\mathbf{C} = \begin{bmatrix} 1 & 2 \\ 0 & 1 \\ 1 & 0 \\ 0 & 2 \\ 1 & 1 \end{bmatrix} \begin{matrix} \text{PdI}_2 \\ \text{HI} \\ \text{Pd} \\ \text{I}_2 \\ \text{IPdR} \end{matrix}. \quad (10)$$

From Eq. (10), two conservation constraints can be derived as shown in Eqs. (11) and (12),

$$[\text{PdI}_2] + [\text{Pd}] + [\text{IPdR}] = [\text{Pd}_{\text{tot}}] = [\text{PdI}_2]_0 + [\text{Pd}]_0 + [\text{IPdR}]_0, \quad (11)$$

$$2[\text{PdI}_2] + [\text{HI}] + 2[\text{I}_2] + [\text{IPdR}] = [\text{I}_{\text{tot}}] = 2[\text{PdI}_2]_0 + [\text{HI}]_0 + 2[\text{I}_2]_0 + [\text{IPdR}]_0. \quad (12)$$

Equation (11) illustrates the preservation of the overall palladium content, while Eq. (12) shows the conservation of iodine within the system.

The subsequent procedure involves the computation of matrix \mathbf{E} and the identification of relevant reaction pathways (steady-state subnetworks). The expression for matrix \mathbf{E} is given by Eq. (13) (calculation details are provided in Appendix III in the supplementary material),

$$\mathbf{E} = \begin{bmatrix} 0 & 1 & 1 \\ 0 & 1 & 1 \\ 0 & 1 & 0 \\ 0 & 0 & 1 \\ 1 & 0 & 0 \\ 1 & 0 & 0 \end{bmatrix} \begin{matrix} \text{R}_1 \\ \text{R}_2 \\ \text{R}_3 \\ \text{R}_4 \\ \text{R}_5 \\ \text{R}_{-5} \end{matrix}. \quad (13)$$

Matrix \mathbf{E} was found to have three columns where the first column represents the equilibrium pathways E_1 [(R_5) and (R_{-5})], consisting only of a pair of reversible reactions. The second and third columns include irreversible reactions E_2 [(R_1), (R_2), and (R_3)] and E_3 [(R_1), (R_2), and (R_4)], respectively.

Using Eq. (4), the reaction rates at steady state were expressed as a linear combination of current rates [see Eq. (14)],

$$\begin{aligned} r_{\text{ss},1} &= j_2 + j_3, \\ r_{\text{ss},2} &= j_2 + j_3, \\ r_{\text{ss},3} &= j_2, \\ r_{\text{ss},4} &= j_3, \\ r_{\text{ss},5} &= j_1, \\ r_{\text{ss},6} &= j_1. \end{aligned} \quad (14)$$

To assess the possible presence of an unstable steady state and identify key intermediate species, we analyzed the diagonal minors of matrix $\mathbf{V}(\mathbf{j})$. Two negative diagonal minors were discovered with dimensions 3×3 . The first minor includes the intermediate species PdI₂, HI, and Pd, while the second minor consists of PdI₂, HI, and I₂. These two diagonal minors play a crucial role in generating instabilities within the model. Specifically, destabilizing feedback cycles are formed due to interactions between these aforementioned species. The expressions for the determinants of these considered diagonal minors are as follows:

$$\beta_{\text{PdI}_2, \text{HI}, \text{Pd}} = -2j_1(j_2 + j_3)^2, \quad (15)$$

$$\beta_{\text{PdI}_2, \text{HI}, \text{I}_2} = -2j_1(j_2 + j_3)^2. \quad (16)$$

Interestingly, the expressions for both diagonal minors are the same. The current j_1 in combination with either j_2 or j_3 is required for instabilities to exist in this model, since removing any two currents leads to cancellation of negative terms in Eqs. (15) and (16). Different types of bifurcations present in the model were identified by analyzing the coefficients of the characteristic polynomial. Analyses of α_1 – α_3 have shown that there are negative terms only in α_3 , while α_4 and α_5 are zeros as a consequence of the conservation constraints [Eqs. (11) and (12)]. The expression for α_3 is presented in Eq. (17), where the reciprocal steady-state concentrations h_1 – h_5 correspond to the reciprocal values of PdI₂, HI, Pd, I₂, and IPdR, respectively,

$$\alpha_3 = h_1 j_1 (j_2 + j_3)^2 (4h_2 h_5 + h_4 h_5 - 2h_2 h_3 - h_2 h_4). \quad (17)$$

In Eq. (17), h_1 – h_5 correspond to reciprocal steady-state concentrations of PdI₂, HI, Pd, I₂ and IPdR, respectively. The existence of a negative term solely in α_3 implies that this system can only undergo a saddle-node (SN) bifurcation. The exact condition for the appearance of the SN bifurcation ($\alpha_3 = 0$) was derived from Eq. (17) and shown in Eq. (18),

$$h_5 = \frac{2h_3 + h_4}{4h_2 + h_4} h_2. \quad (18)$$

If the value of h_5 exceeds the threshold defined by Eq. (18), α_3 is positive, which indicates a stable steady state. On the contrary, if h_5 falls below the threshold, α_3 is negative and signals an unstable steady state. Equation (17) shows that the stability condition is valid only when both h_1 and j_1 are greater than zero, and this must be accompanied by either j_2 or j_3 being also greater than zero. In other words, PdI₂ must be present in the system for instability to occur, along with reactions found in E_1 together with reactions from either E_2 or E_3 . The negativity of α_3 is determined solely by the ratio between h_2 , h_3 , h_4 , and h_5 . Two extreme scenarios result in α_3 becoming negative: when the value of h_4 is negligible compared to

h_3 , thereby leading to specific stability conditions,

$$\begin{aligned} 2h_5 &< h_3, \\ h_4 h_5 &< 2h_2 h_3, \end{aligned} \quad (19)$$

and when h_4 is higher than h_3 , which results in the second system of inequalities,

$$\begin{aligned} 4h_5 &< h_4, \\ h_5 &< h_2. \end{aligned} \quad (20)$$

Based on the analysis of Eqs. (18)–(20), it can be deduced that instabilities in this model arise when the value of h_5 is lower than that of h_2 . In other words, a higher steady-state concentration of [IPdR] compared to [HI] leads to instability. This phenomenon can be attributed to the autocatalysis of HI in reaction (R₁), which serves as the main driving force behind these instabilities within the model. Notably, for instabilities to occur, reactions from either of subnetworks E_2 and E_3 [specifically (R₂), (R₃), and (R₄)] must also be present. Additionally, both reaction (R₅) and its reverse counterpart (R₋₅), found in subnetwork E_1 , are essential for triggering instabilities within this model. Sustaining the occurrence of these reactions is crucial for maintaining the destabilizing feedback cycle, thus requiring high concentrations of IPdR.

B. Numerical validation of the model

To validate the derived equations and stability conditions, a numerical analysis was performed. The reaction rate constants reported in the study that proposed reaction network presented in Table I²⁵ were reapplied to ensure consistency. Table II displays the values of these parameters.

By using Eqs. (11), (12), and (14), the steady-state equation for HI was solved while expressing the steady-state concentrations of the other species and current rates j_1 – j_3 as functions of HI. The solution revealed that the steady-state concentration of HI can be obtained by solving a fourth-degree polynomial provided in the supplementary material [Eq. (A1.3), Appendix I]. In this analysis, we used an initial concentration of PEGA, denoted as [PEGA]₀, as a continuation parameter which, as an initial concentration of the substrate, can be adjusted in the experimental work. Figure 1 shows the results obtained from this analysis.

On examination of the values of \mathbf{j} parameters derived from Eq. (14), it was observed that for the rate constant values defined in Table II, the behavior of the reaction network is primarily determined by the reactions in the subnetworks E_1 and E_3 [(R₁), (R₂), (R₄), (R₅), and (R₋₅)]. This observation arises from the significantly lower value of j_2 compared to those of j_1 and j_3 . Figure 2 depicts the dependence of parameters j_1 to j_3 on the initial concentration of [PEGA]₀.

TABLE II. The values of reaction rate constants used in the analysis.²⁵

$k_1/\text{M}^{-3} \text{min}^{-1}$	$k_2/\text{M}^{-1} \text{min}^{-1}$	$k_3/\text{M}^{-1} \text{min}^{-1}$	$k_4/\text{M}^{-2} \text{min}^{-1}$	k_5/min^{-1}	$k_{-5}/\text{M}^{-1} \text{min}^{-1}$
6.00×10^{12}	2.00×10^3	1.00×10^{-7}	2.00×10^7	3.00×10^{-4}	1.00×10^2

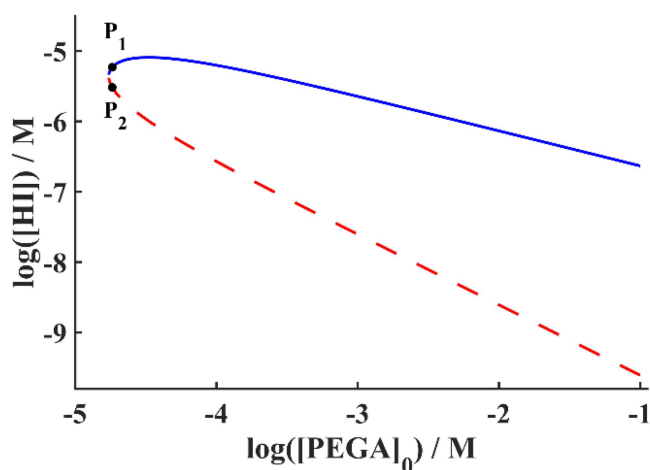


FIG. 1. Bifurcation diagram obtained using methods of numerical continuation with $[\text{PEGA}]_0$ as a control parameter. The values of the reaction rate constants used in the analysis are presented in Table II; the blue line represents a stable steady state, while the red line represents an unstable steady state.

The analysis reveals that the system indeed undergoes an SN bifurcation, leading to two branches of solutions. One branch consists of stable steady states, while the other branch includes unstable states. It is also worth noting that under the same parameter values, a steady state can be stable or unstable depending on its initial conditions (the value of $[\text{PEGA}]_0$). Numerical simulations were performed to investigate the system's behavior. The reaction rate constants corresponded to those found in Table II, while the initial conditions matched the steady-state concentrations at points P_1 and P_2 in Fig. 1. The results of the numerical simulations corresponding to the case of stable and unstable steady-state are presented in Fig. 3.

Previous study²⁵ has shown that the model can produce oscillatory dynamics. Although our analysis has shown that the Andronov–Hopf bifurcation cannot be obtained within this reaction network, we managed to obtain damped oscillatory dynamics in numerical simulations. The ability to create an Andronov–Hopf bifurcation is a useful approach for generating oscillatory dynamics.

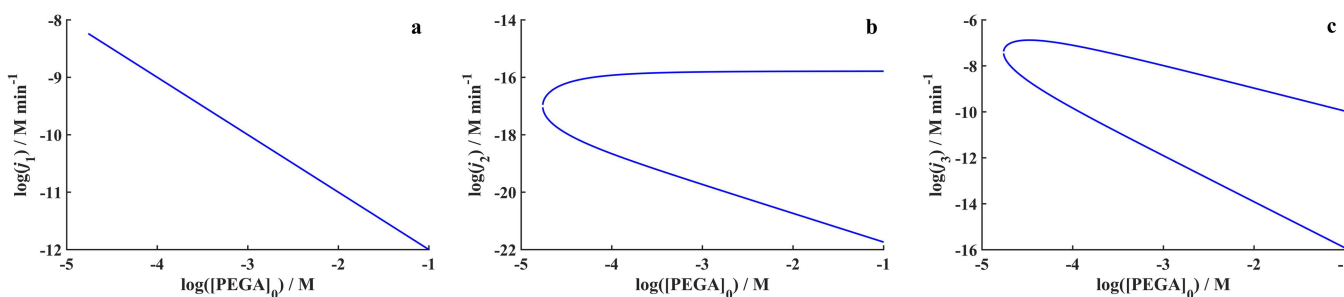


FIG. 2. The values of current rates (a) j_1 , (b) j_2 , and (c) j_3 , as a function of the values of initial concentration of $[\text{PEGA}]_0$. Values of current rates j_1 – j_3 were calculated from Eq. (14) for the values of steady-state concentrations presented in Fig. 1.

It enables the simulation of sustained oscillations with controllable characteristics and the efficient determination of conditions for its emergence. Hence, further modifications to the proposed reaction network, such as the introduction of additional reactions, are necessary to enhance the flexibility of the model and its effectiveness in capturing the complexities found experimentally. An example of oscillatory dynamics obtained in the model is presented in Fig. 4.

C. Stability analysis in the presence of diffusion

Stability analysis was conducted by examining the coefficients of the characteristic polynomial defined in Eqs. (21)–(23). Within $\alpha_{3,RD}$, $\alpha_{4,RD}$, and $\alpha_{5,RD}$, negative terms capable of generating instabilities were found. The expressions for $\alpha_{3,RD}$, $\alpha_{4,RD}$, and $\alpha_{5,RD}$ are as follows:

$$\alpha_{3,RD} = \alpha_3 + p(\omega, \mathbf{D}, \mathbf{j}, \mathbf{h}), \quad (21)$$

$$\alpha_{4,RD} = q(\omega, \mathbf{D}, \mathbf{j}, \mathbf{h}), \quad (22)$$

$$\alpha_{5,RD} = z(\omega, \mathbf{D}, \mathbf{j}, \mathbf{h}), \quad (23)$$

where α_3 corresponds to the coefficients of the characteristic polynomial of the spatially uniform system [for α_3 , see Eq. (17)], while $p(\omega, \mathbf{D}, \mathbf{j})$, $q(\omega, \mathbf{D}, \mathbf{j})$, and $z(\omega, \mathbf{D}, \mathbf{j})$ are multivariate polynomials in ω , D_1 – D_5 , j_1 – j_3 , and h_1 – h_5 . In the case of $\alpha_{4,RD}$ and $\alpha_{5,RD}$, there are only reaction–diffusion related terms since α_4 and α_5 are zeros due to the presence of conservation constraints in the case of a spatially uniform system [see Eqs. (11) and (12)]. The expressions for $p(\omega, \mathbf{D}, \mathbf{j})$, $q(\omega, \mathbf{D}, \mathbf{j})$, and $z(\omega, \mathbf{D}, \mathbf{j})$ can be found in the supplementary material [Eqs. (A2.1)–(A2.14), Appendix II].

D. Analysis of $\alpha_{3,RD}$

The analysis of $p(\omega, \mathbf{D}, \mathbf{j}, \mathbf{h})$ has shown that only positive terms can be found there. For instabilities to occur through $\alpha_{3,RD} < 0$, it is possible only if the steady state of a spatially uniform system is already unstable ($\alpha_3 < 0$) while $p(\omega, \mathbf{D}, \mathbf{j}, \mathbf{h}) > 0$. Hence, essential conditions for the system to undergo unstable steady state are determined by Eqs. (18)–(20). Furthermore, the instabilities in this scenario arise from destabilizing feedback cycles within the reaction network. Diffusion, on the other hand, acts as a stabilizer for steady-state and helps us to propagate these instabilities across the system.

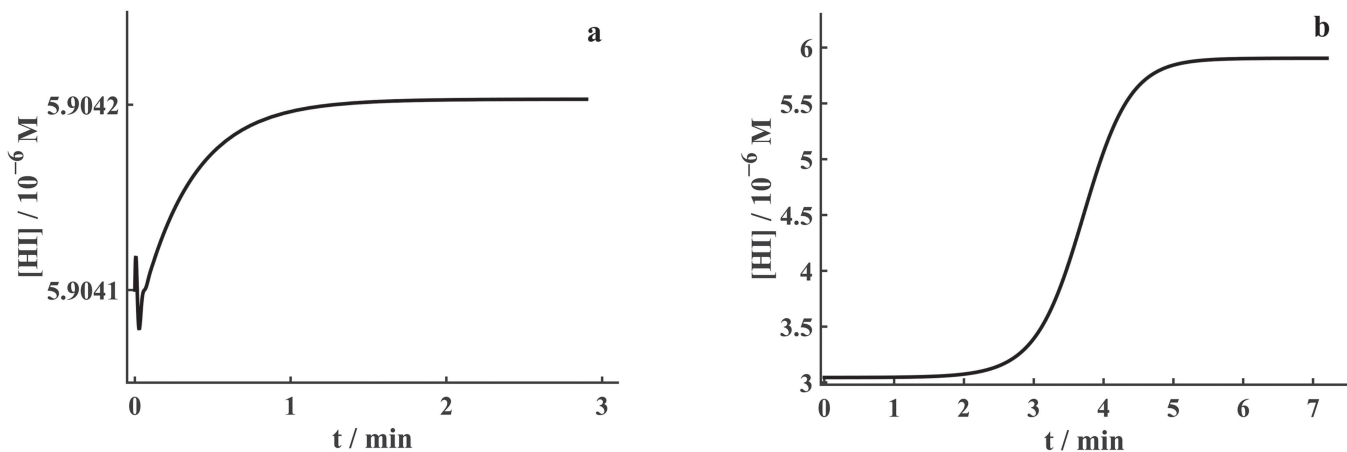


FIG. 3. Numerical simulations of the reaction network presented in Table I: (a) stable steady state corresponding to points P_1 with initial conditions $[\text{PdI}_2]_0 = 1.82 \times 10^{-5}$ M, $[\text{HI}]_0 = 5.90 \times 10^{-6}$ M, $[\text{Pd}]_0 = 1.30 \times 10^{-5}$ M, $[\text{I}_2]_0 = 1.50 \times 10^{-5}$ M, and $[\text{IPdR}]_0 = 9.26 \times 10^{-6}$ M; (b) unstable steady state corresponding to point P_2 with initial conditions $[\text{PdI}_2]_0 = 1.82 \times 10^{-5}$ M, $[\text{HI}]_0 = 3.04 \times 10^{-6}$ M, $[\text{Pd}]_0 = 4.32 \times 10^{-6}$ M, $[\text{I}_2]_0 = 1.18 \times 10^{-5}$ M, and $[\text{IPdR}]_0 = 1.80 \times 10^{-5}$ M; the values of reaction rate constants used in both cases are presented in Table II. In both cases, the value of $[\text{PEGA}]_0 = 1.83 \times 10^{-5}$ M was used.

To verify the applicability of Eqs. (18)–(20) to a spatially non-uniform system, numerical simulations were conducted. Parameters were selected to represent a scenario where the steady state of the spatially uniform system is already unstable (point P_2 on the bifurcation diagram Fig. 1). To ensure that the unstable steady state originates only from $\alpha_3 < 0$, parameter values were adjusted so that both $\alpha_{4,\text{RD}}$ and $\alpha_{5,\text{RD}}$ [Eqs. (22) and (23)] produce positive values. This was achieved by modifying the diffusion coefficients D_1 – D_5 while keeping all other parameters unchanged. The values of the

reaction rate constants used in the simulations are presented in Table II. The results of the simulations, together with the parameter values used, are presented in Fig. 5 (multimedia available online).

It was observed that when an initial perturbation is induced at the center of the computational domain, a front is formed and moves toward the boundaries at a constant velocity. As the front advances, there is a gradual increase in the concentration of hydrogen iodide HI. Upon reaching the boundaries of the computational domain, the concentration of HI begins to increase throughout the entire area. In particular, the rate of increase is more pronounced near the boundaries compared to the central region where the initial perturbation was introduced. This fast increase continues until a uniform distribution of the concentration is achieved throughout the entirety of the domain.

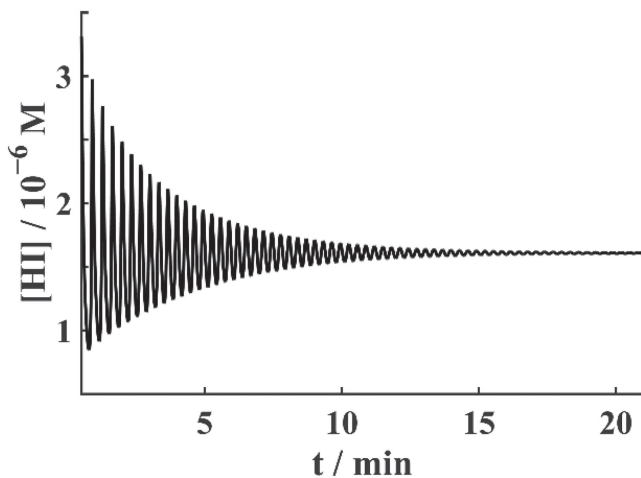


FIG. 4. Numerical simulation of the oscillatory dynamics obtained in the model under consideration. The values of reaction rate constants used in the simulations are presented in Table II while $[\text{PEGA}]_0 = 2.03 \times 10^{-5}$ M; initial conditions used in the simulations: $[\text{PdI}_2]_0 = 4.05 \times 10^{-5}$ M; $[\text{HI}]_0 = 0$ M; $[\text{Pd}]_0 = 0$ M; $[\text{I}_2]_0 = 0$ M; and $[\text{IPdR}]_0 = 0$ M.

E. Analysis of $\alpha_{4,\text{RD}}$ and $\alpha_{5,\text{RD}}$

In a spatially uniform system, it was shown that α_4 and α_5 (both equal to 0) do not contribute to the steady stability of the reaction network considered. The introduction of diffusion changes this by creating the terms in the expansions for $\alpha_{4,\text{RD}}$ and $\alpha_{5,\text{RD}}$ that are the result of the interaction between diffusion and reactions. Now, both $\alpha_{4,\text{RD}}$ and $\alpha_{5,\text{RD}}$ determine steady-state stability, as shown clearly in Eqs. (11) and (12), which can lead to the emergence of diffusion-driven instabilities. Therefore, analysis of $\alpha_{4,\text{RD}}$ and $\alpha_{5,\text{RD}}$ was conducted.

The analysis of $\alpha_{4,\text{RD}}$ [Eq. (22)] revealed that all negative terms are contained within the coefficient $q_{1,4}(\omega, \mathbf{D}, \mathbf{j}, \mathbf{h})$ presented in Eq. (24),

$$q_{1,4}(\mathbf{D}, \mathbf{j}, \mathbf{h}) = h_1 j_1 (j_2 + j_3)^2 (4D_3 h_2 h_5 - 2D_4 h_2 h_3 - D_3 h_2 h_4 - 2D_5 h_2 h_3 + D_2 h_4 h_5 + 4D_4 h_2 h_5 - D_5 h_2 h_4 + D_3 h_4 h_5). \quad (24)$$

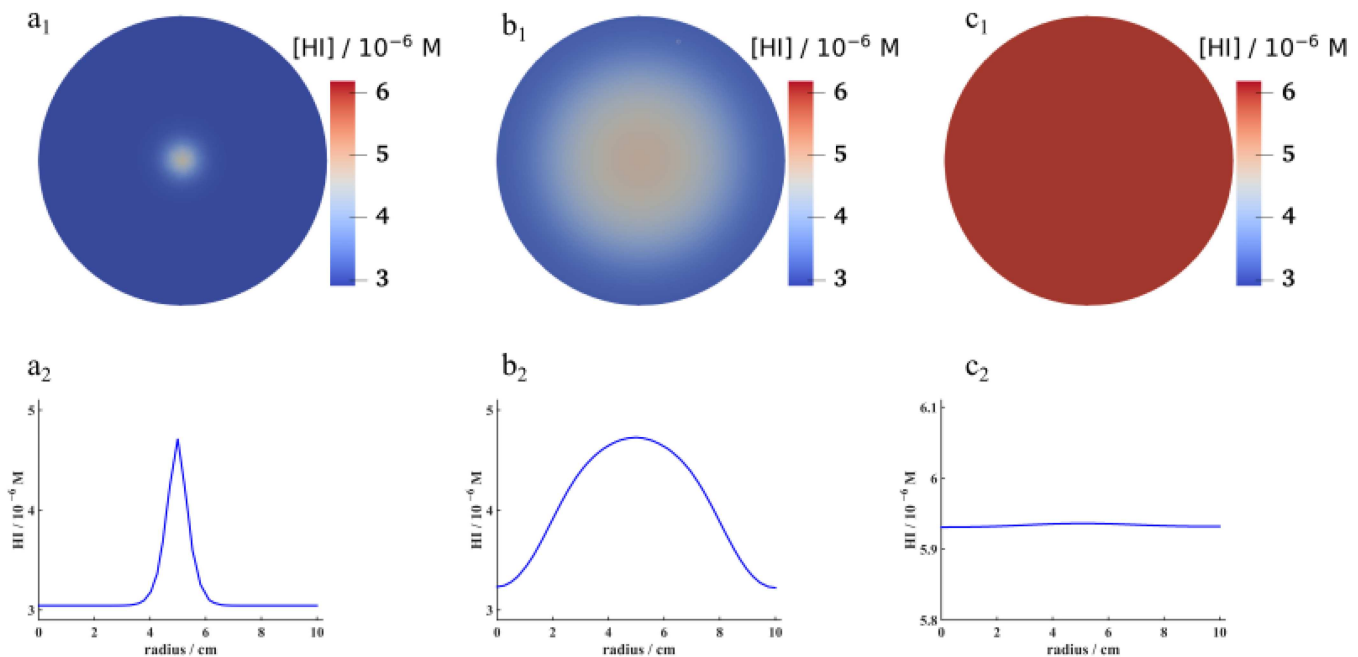


FIG. 5. Numerical simulations obtained for $\alpha_3 < 0$ while $\alpha_{4,RD} > 0$ and $\alpha_{5,RD} > 0$. Figures a₁–c₁ represent the change of HI concentration in the computational domain over time: (a) $t = 1.53 \times 10^3$ min, (b) 1.48×10^4 min, and (c) 1.00×10^5 min. Figures a₂–c₂ represent the change in HI concentration measured between points (0 cm, 0 cm) and (10 cm, 0 cm). Parameters used in simulations: for the values of the reaction rate, constants are presented in Table II: $[PEGA]_0 = 1.832 \times 10^{-5}$ M, $D_1 = 1.00 \times 10^{-5}$ cm² s⁻¹, $D_2 = 1.00 \times 10^{-4}$ cm² s⁻¹, $D_3 = 1.00 \times 10^{-4}$ cm² s⁻¹, $D_4 = 1.80 \times 10^{-5}$ cm² s⁻¹, and $D_5 = 1.80 \times 10^{-5}$ cm² s⁻¹; initial conditions throughout the domain except in the center of the computational domain: $[PdI_2]_0 = 1.82 \times 10^{-5}$ M, $[HI]_0 = 3.04 \times 10^{-6}$ M, $[Pd]_0 = 4.32 \times 10^{-6}$ M, $[I_2]_0 = 1.18 \times 10^{-5}$ M, $[IPdR]_0 = 1.80 \times 10^{-5}$ M; perturbation was introduced in the center of the computational domain where the initial concentrations were set to be: $[PdI_2]_0 = 3.64 \times 10^{-5}$ M, $[HI]_0 = 6.08 \times 10^{-6}$ M, $[Pd]_0 = 8.64 \times 10^{-6}$ M, $[I_2]_0 = 2.36 \times 10^{-5}$ M, and $[IPdR]_0 = 3.60 \times 10^{-5}$ M. Multimedia available online.

The efficient strategy for achieving $\alpha_{4,RD} < 0$ requires two steps: Step (1) identifying conditions under which $q_{1,4}(\omega, \mathbf{D}, \mathbf{j}, \mathbf{h})$ becomes negative and Step (2) finding the parameters that contribute the most to the positive terms in $q(\omega, \mathbf{D}, \mathbf{j}, \mathbf{h})$, thus stabilizing the steady state. Solving Step 1 requires a thorough examination of $q_{1,4}(\omega, \mathbf{D}, \mathbf{j}, \mathbf{h})$. The similarity between $q_{1,4}(\omega, \mathbf{D}, \mathbf{j}, \mathbf{h})$ and the expression of α_3 is apparent. Both depend on the presence of parameters h_1 and j_1-j_3 for instabilities to occur, regardless of their specific values. However, in contrast to α_3 , conditions for $\alpha_{4,RD} < 0$ are influenced by both the ratio between the parameters h_2-h_5 and the diffusion coefficients D_2-D_5 . Additionally, it was observed that only positive terms are linked to h_5 . As a result, a condition for ensuring $q_{1,4}(\omega, \mathbf{D}, \mathbf{j}, \mathbf{h}) < 0$ was obtained,

$$h_5 \leq \frac{D_3 h_4 + 2D_4 h_3 + 2D_5 h_3 + D_5 h_4}{4D_3 h_2 + D_2 h_4 + 4D_4 h_2 + D_3 h_4} h_2. \quad (25)$$

According to Eqs. (A2.6)–(A2.9) (Appendix II in the supplementary material), the diffusion coefficient D_1 for the intermediate species PdI_2 is only found in positive terms of $q(\omega, \mathbf{D}, \mathbf{j}, \mathbf{h})$. This suggests that D_1 plays a significant role in stabilizing the steady state.

The same analysis was also performed on $\alpha_{5,RD}$ [Eq. (23)]. In this case, all negative terms were found within $z_{1,4}(\omega, \mathbf{D}, \mathbf{j}, \mathbf{h})$

[Eq. (26)] while all remaining terms are positive,

$$z_{1,4}(\mathbf{D}, \mathbf{j}, \mathbf{h}) = h_1 j_1 (j_2 + j_3)^2 (D_2 D_3 h_4 h_5 + 4D_3 D_4 h_2 h_5 - D_3 D_5 h_2 h_4 - 2D_4 D_5 h_2 h_3). \quad (26)$$

The condition for $z_{1,4}(\omega, \mathbf{D}, \mathbf{j}, \mathbf{h}) < 0$ was found to be defined by Eq. (27),

$$h_5 \leq \frac{D_5 (D_3 h_4 + 2D_4 h_3)}{D_3 (D_2 h_4 + 4D_4 h_2)} h_2. \quad (27)$$

Equation (27) is similar to Eq. (25), except that it is simpler in the number of terms. As in the previous case, the diffusion coefficient D_1 associated with the intermediate species PdI_2 can only be found among the positive terms of $z(\omega, \mathbf{D}, \mathbf{j}, \mathbf{h})$. It can be concluded from this analysis that the slow diffusion of the PdI_2 catalyst is an important factor that contributes to the appearance of diffusion-driven instabilities. Furthermore, the similarities between Eqs. (24)–(27) and the equations describing stability conditions for spatially uniform systems are evident, indicating that autocatalysis of HI and a destabilizing feedback cycle remain the main driving force for instabilities within this model. The key condition lies in the appropriate difference in concentrations of HI and IPdR. Although the steady-state of a spatially uniform system can be stable ($h_5 > h_2$), under specific diffusion conditions, instability may emerge. Equations (25) and (27) demonstrate that this is most

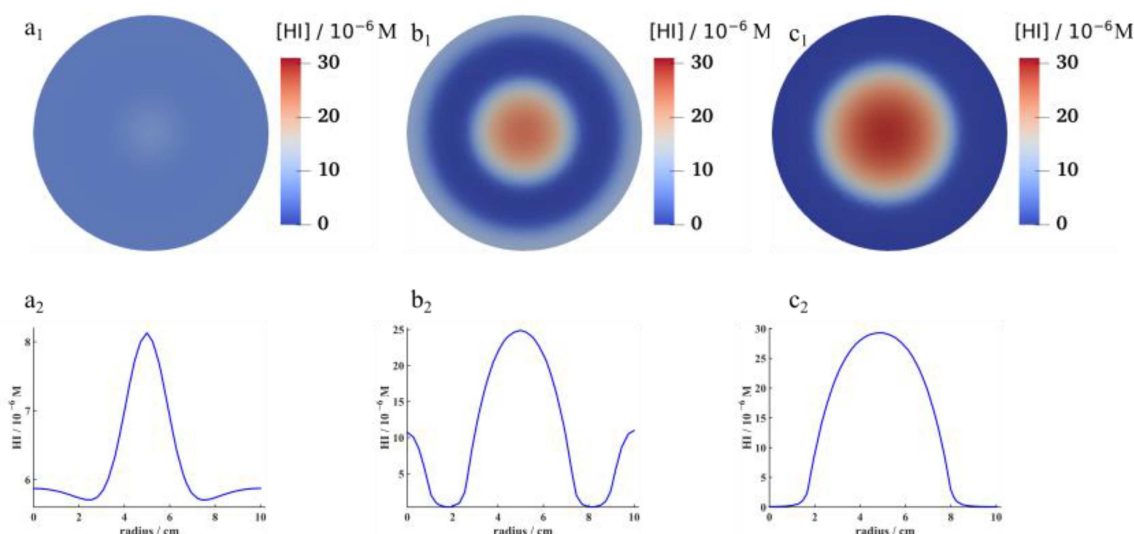


FIG. 6. Numerical simulations obtained for $\alpha_{4,RD} < 0$ and $\alpha_{5,RD} < 0$. Figures a_1 – c_1 represent the change of HI concentration in the computational domain over time: (a) $t = 1.53 \times 10^3$ min, (b) 4.08×10^4 min, and (c) 1.45×10^7 min. Figures a_2 – c_2 represent the change in HI concentration measured between points (0 cm, 0 cm) and (10 cm, 0 cm). Parameters used in simulations: $k_1 = 6.00 \times 10^{12} \text{ M}^{-3} \text{ min}^{-1}$, $k_2 = 2.00 \times 10^3 \text{ M}^{-1} \text{ min}^{-1}$, $k_3 = 1.00 \times 10^{-7} \text{ M}^{-1} \text{ min}^{-1}$, $k_4 = 2.00 \times 10^7 \text{ M}^{-2} \text{ min}^{-1}$, $k_5 = 3.00 \times 10^{-4} \text{ min}^{-1}$, $k_{-5} = 1.00 \times 10^2 \text{ M}^{-1} \text{ min}^{-1}$, $[\text{PEGA}]_0 = 1.83 \times 10^{-5} \text{ M}$, $D_1 = 1.00 \times 10^{-5} \text{ cm}^2 \text{ s}^{-1}$, $D_2 = 1.00 \times 10^{-4} \text{ cm}^2 \text{ s}^{-1}$, $D_3 = 2.00 \times 10^{-5} \text{ cm}^2 \text{ s}^{-1}$, $D_4 = 1.00 \times 10^{-4} \text{ cm}^2 \text{ s}^{-1}$, and $D_5 = 1.20 \times 10^{-3} \text{ cm}^2 \text{ s}^{-1}$; initial conditions throughout the domain except in the center of the computational domain: $[\text{PdI}_2]_0 = 1.82 \times 10^{-5} \text{ M}$, $[\text{HI}]_0 = 5.90 \times 10^{-6} \text{ M}$, $[\text{Pd}]_0 = 1.30 \times 10^{-5} \text{ M}$, $[\text{I}_2]_0 = 1.50 \times 10^{-5} \text{ M}$, and $[\text{IPdR}]_0 = 9.26 \times 10^{-6} \text{ M}$; perturbation was introduced in the center of computational domain, where initial concentration were set to be: $[\text{PdI}_2]_0 = 3.64 \times 10^{-5} \text{ M}$, $[\text{HI}]_0 = 1.18 \times 10^{-5} \text{ M}$, $[\text{Pd}]_0 = 2.60 \times 10^{-5} \text{ M}$, $[\text{I}_2]_0 = 3.00 \times 10^{-5} \text{ M}$, and $[\text{IPdR}]_0 = 1.85 \times 10^{-5} \text{ M}$. Multimedia available online.

likely when diffusion of IPdR occurs faster compared to other intermediate species, leading to variations in concentration levels and consequent instability emergence.

To test the validity of Eqs. (25) and (27), numerical analysis was employed. Simulations were carried out under conditions corresponding to a stable steady state in a spatially uniform system, specifically resembling point P_1 as shown in Fig. 1. To ensure that Eqs. (25) and (27) were satisfied, different diffusion coefficient values were tested while maintaining constant values for intermediate species concentrations and reaction rate constants as those defined in point P_1 . The numerical analysis revealed that $\alpha_{4,RD} > 0$ and $\alpha_{5,RD} < 0$ were achievable under the given conditions. However, it was not possible to achieve a situation where $\alpha_{4,RD} < 0$ and $\alpha_{5,RD} > 0$. Additionally, both $\alpha_{4,RD}$ and $\alpha_{5,RD}$ could be negative, which was used as the scenario for subsequent simulations. The simulation results, along with the parameter values used, are presented in Fig. 6 (multimedia available online).

After the initial perturbation, a front begins to emerge and moves toward the boundaries of the computational domain. This results in regions of both lower and higher HI concentrations becoming apparent. The areas with higher HI concentrations are situated near both the boundaries and the center of the computational domain, while those with lower HI concentrations are located between them. Over time, regions with higher HI concentrations near the boundaries gradually disappear. As a result, only areas with lower HI concentration and those with higher HI concentration near the center of the computational domain remain. Additional 1D numerical simulations performed on much longer timescale also

confirmed that observed regions of lower and higher HI concentrations represent permanent structures (see Appendix IV in the supplementary material).

V. CONCLUSIONS

The study focuses on the dynamics of the reaction network of the oscillatory carbonylation reaction using poly(ethylene glycol) methyl ether acetylene (PEGA) under pseudo-batch conditions. To assess steady-state stability, we utilized stoichiometric network analysis in both spatially uniform and non-uniform systems. In a spatially uniform system, two destabilizing feedback cycles were identified as contributing to unstable steady states: one involving PdI₂, HI, and Pd, and another involving PdI₂, HI, and I₂. The analysis of a spatially uniform system has shown that the proposed model can simulate saddle-node bifurcation when the concentration of IPdR exceeded that of other species. This result was confirmed by bifurcation analysis and numerical simulations. In addition, numerical analysis has also indicated that dampened oscillatory dynamics can be generated in the analyzed reaction network, although simulation of the Andronov–Hopf bifurcation is not possible. To obtain the Andronov–Hopf bifurcation, which is a preferred method for achieving oscillatory dynamics in reaction networks since it allows easier control of the characteristics of oscillatory dynamics, additional reactions must be incorporated into the model.

In contrast to these findings, by introducing diffusion into the system, two types of instabilities were observed. The first type occurred in an already unstable spatially uniform system, and its

emergence was determined by conditions for SN bifurcation. In this case, an expanding reaction–diffusion front was observed in the system. The second type, known as Turing patterns, occurred when a stable spatially uniform system became destabilized as a result of diffusion. Interestingly, it was found that slower PdI_2 diffusion played a crucial role in inducing diffusion-driven instabilities, since PdI_2 typically stabilizes the steady state. Numerical simulations confirmed the validity of these derived conditions for both types of instabilities, supporting the effectiveness and potential applicability of this model for further investigation. PdI_2 has a role of the catalyst in the system, and while in the studied model, it is presented as the reacting species, due to its poor solubility in methanol, it is actually used in the presence of KI leading to the formation of the complex PdI_4^{2-} ,⁵⁹ which acts as the catalyst in this system. However, since the oscillations in turbidity, experimentally captured in this oscillatory system, have been linked with the precipitations of $\text{Pd}(0)$ and its cycling to Pd^{+2} [as summarized by (R_1) , (R_3) , and (R_4) in the model, Table I],²⁵ regions of higher and lower concentrations of Pd^{+2} can be envisioned as a consequence of the difference in the solubility of Pd species involved in this system. Furthermore, with progress in studies of oscillatory carbonylation reactions and the introduction of both the polymeric substrate and the polymeric catalyst,^{35,60} diffusion could be altered by the change in the size of the species involved in this system, offering additional opportunities to introduce the instability to the system. Using the study reported here as a basis, experimental studies are planned, seeking to uncover complexities not yet seen in oscillatory carbonylation reactions, which potentially can lead to discoveries, understanding, and utilization of patterns seen in nature but not yet understood or applied.

The results of this study also indicate that diffusion-driven instabilities can emerge in reaction networks only if destabilizing feedback cycles are present within the network. In other words, they will emerge only if instabilities can be found in spatially uniform systems. This seems to be a general characteristic of reaction networks, which is also consistent with the results of our previous work.³⁷ A significant result related to conservation constraints was also found. In a spatially uniform system, instability conditions were defined by $\alpha_1-\alpha_3$ while $\alpha_4-\alpha_5$ are zero due to the conservation constraints. The presence of diffusion maintains the satisfaction of conservation constraints as confirmed by expressions for $\alpha_{4,\text{RD}}$ and $\alpha_{5,\text{RD}}$, but in this scenario, $a_{4\text{rd}}$ and $a_{5\text{rd}}$ become important for determining instability conditions due to the interaction between chemical reactions and diffusion. Furthermore, our numerical simulations also revealed that the time for the occurrence of diffusion-driven instabilities (Fig. 6) is considerably longer than the time for the emergence of instabilities when a spatially uniform system is already unstable (Fig. 5). This could potentially explain why diffusion-driven instabilities are rarely observed in experimental studies; their emergence may require a longer time period than typically observed in laboratory settings.

SUPPLEMENTARY MATERIAL

See the supplementary material for Appendix I: equations used within this paper to calculate steady-state concentrations; Appendix II: expressions for multivariate polynomials $p(\omega, \mathbf{D}, \mathbf{j})$, $q(\omega, \mathbf{D}, \mathbf{j})$, and $z(\omega, \mathbf{D}, \mathbf{j})$ associated with coefficients of the

characteristic polynomial defined in Eqs. (21)–(23); Appendix III: algorithm and instructions how to calculate matrices E and C; and Appendix IV: results from 1D numerical simulation.

ACKNOWLEDGMENTS

This work was supported by the Ministry of Science, Technological Development and Innovation of the Republic of Serbia (Contract No. 451-03-66/2024-03/200146) and the Science Fund of the Republic of Serbia (Grant No. 7743504, Physicochemical aspects of rhythmicity in neuroendocrine systems: Dynamic and kinetic investigations of underlying reaction networks and their main compounds, NES). In addition to Science Fund of the Republic of Serbia (grant number 7743504), as detailed in the Acknowledgements, this work was also supported by the Ministry of Science, Technological Development and Innovation of the Republic of Serbia (contract number 451-03-66/2024-03/200146).

AUTHOR DECLARATIONS

Conflict of Interest

The authors have no conflicts to disclose.

Author Contributions

Stevan Maćešić: Conceptualization (lead); Formal analysis (lead); Funding acquisition (lead); Investigation (lead); Methodology (lead); Software (lead); Validation (equal); Visualization (lead); Writing – original draft (equal); Writing – review & editing (equal). **Katarina Novakovic:** Writing – original draft (equal); Writing – review & editing (equal).

DATA AVAILABILITY

The data that support the findings of this study are available within the article and its supplementary material.

REFERENCES

- ¹A. M. Turing, “The chemical basis of morphogenesis,” *Bull. Math. Biol.* **52**, 153–197 (1990).
- ²A. Gierer and H. Meinhardt, “A theory of biological pattern formation,” *Kybernetik* **12**, 30–39 (1972).
- ³S. Kondo and R. Asai, “A reaction–diffusion wave on the skin of the marine angelfish *Pomacanthus*,” *Nature* **376**, 765–768 (1995).
- ⁴E. Dulos, J. Boissonade, J. Perraud, B. Rudovics, and P. De Kepper, “Chemical morphogenesis: Turing patterns in an experimental chemical system,” *Acta Biotheor.* **44**, 249–261 (1996).
- ⁵A. Badugu, C. Kraemer, P. Germann, D. Menshykau, and D. Iber, “Digit patterning during limb development as a result of the BMP-receptor interaction,” *Sci. Rep.* **2**, 991 (2012).
- ⁶S. Getzin, H. Yizhaq, B. Bell, T. Erickson, A. Postle, I. Katra *et al.*, “Discovery of fairy circles in Australia supports self-organization theory,” *Proc. Natl. Acad. Sci. U.S.A.* **113**, 3551–3556 (2016).
- ⁷K. Kaiser, B. McGlynn, and R. Emanuel, “Ecohydrology of an outbreak: Mountain pine beetle impacts trees in drier landscape positions first,” *Ecohydrology* **6**, 444–454 (2012).
- ⁸L. Alencar, M. I. S. Escada, and J. L. C. Camargo, “Forest regeneration pathways in contrasting deforestation patterns of Amazonia,” *Front. Environ. Sci.* **11**, 991695 (2023).
- ⁹D. Menshykau, O. Michos, C. Lang, L. Conrad, A. P. McMahon, and D. Iber, “Image-based modeling of kidney branching morphogenesis reveals GDNF-RET

- based Turing-type mechanism and pattern-modulating WNT11 feedback," *Nat. Commun.* **10**, 239 (2019).
- ¹⁰A. Nakamasu, G. Takahashi, A. Kanbe, and S. Kondo, "Interactions between zebrafish pigment cells responsible for the generation of Turing patterns," *Proc. Natl. Acad. Sci. U.S.A.* **106**, 8429–8434 (2009).
- ¹¹M. Rietkerk, S. C. Dekker, P. C. de Ruiter, and J. van de Koppel, "Self-organized patchiness and catastrophic shifts in ecosystems," *Science* **305**, 1926–1929, (2004).
- ¹²G. Theraulaz, E. Bonabeau, S. C. Nicolis, R. V. Solé, V. Fourcassié, S. Blanco *et al.*, "Spatial patterns in ant colonies," *Proc. Natl. Acad. Sci. U.S.A.* **99**, 9645–9649 (2002).
- ¹³S. Kondo, M. Watanabe, and S. Miyazawa, "Studies of Turing pattern formation in zebrafish skin," *Philos. Trans. R. Soc., A* **379**, 20200274 (2021).
- ¹⁴W. Horsthemke and P. Moore, "Turing instability in inhomogeneous arrays of diffusively coupled reactors," *J. Phys. Chem. A* **108**, 2225–2231 (2004).
- ¹⁵R. T. Liu, S. S. Liaw, and P. K. Maini, "Two-stage Turing model for generating pigment patterns on the leopard and the jaguar," *Phys. Rev. E* **74**, 011914 (2006).
- ¹⁶I. R. Epstein and J. A. Pojman, *An Introduction to Nonlinear Chemical Dynamics: Oscillations, Waves, Patterns, and Chaos* (Oxford University Press, 1998).
- ¹⁷I. R. Epstein and K. Showalter, "Nonlinear chemical dynamics: Oscillations, patterns, and chaos," *J. Phys. Chem.* **100**, 13132–13147 (1996).
- ¹⁸A. S. Mikhailov and K. Showalter, "Control of waves, patterns and turbulence in chemical systems," *Phys. Rep.* **425**, 79–194 (2006).
- ¹⁹A. T. Winfree, "Stably rotating patterns of reaction and diffusion," in *Theoretical Chemistry, Periodicities in Chemistry and Biology*, edited by H. Eyring and D. Henderson (Academic Press, 1978), pp. 1–51.
- ²⁰P. De Kepper, V. Castets, E. Dulos, and J. Boissonade, "Turing-type chemical patterns in the chlorite-iodide-malonic acid reaction," *Physica D* **49**, 161–169 (1991).
- ²¹V. Castets, E. Dulos, J. Boissonade, and P. De Kepper, "Experimental evidence of a sustained standing Turing-type nonequilibrium chemical pattern," *Phys. Rev. Lett.* **64**, 2953 (1990).
- ²²J. Carballido-Ladeira, V. K. Vanag, and I. R. Epstein, "Patterns in the Belousov–Zhabotinsky reaction in water-in-oil microemulsion induced by a temperature gradient," *Phys. Chem. Chem. Phys.* **12**, 3656–3665 (2010).
- ²³J. Horváth, I. Szalai, and P. De Kepper, "An experimental design method leading to chemical Turing patterns," *Science* **324**, 772–775 (2009).
- ²⁴L. Yuan, H. Wang, C. Meng, Z. Cheng, X. Lv, and Q. Gao, "Multiple iodide autocatalysis paths of chemo-hydrodynamical patterns in the Briggs–Rauscher reaction," *Phys. Chem. Chem. Phys.* **25**, 13183–13188 (2023).
- ²⁵L. Donlon and K. Novakovic, "Oscillatory carbonylation using alkyne-functionalised poly(ethylene glycol)," *Chem. Commun.* **50**, 15506–15508 (2014).
- ²⁶A. V. Malashkevich, L. G. Bruk, and O. N. Temkin, "New oscillating reaction in catalysis by metal complexes: A mechanism of alkyne oxidative carbonylation," *J. Phys. Chem. A* **101**, 9825–9827 (1997).
- ²⁷C. Grosjean, K. Novakovic, S. K. Scott, A. Whiting, M. J. Willis, and A. R. Wright, "Product identification and distribution from the oscillatory versus non-oscillatory palladium(II) iodide-catalysed oxidative carbonylation of phenylacetylene," *J. Mol. Catal. A: Chem.* **284**, 33–39 (2008).
- ²⁸J. Parker and K. Novakovic, "Influence of water and the reactant addition sequence on palladium(II) iodide-catalyzed phenylacetylene carbonylation," *Ind. Eng. Chem. Res.* **52**, 2520–2527 (2013).
- ²⁹S. N. Gorodskii, A. N. Zakharov, A. V. Kulik, L. G. Bruk, and O. N. Temkin, "Oxidative carbonylation of alkynes in an oscillation mode: I. Concentration limits for oscillations in the course of phenylacetylene carbonylation and possible mechanisms of the process," *Kinet. Catal.* **42**, 251–263 (2001).
- ³⁰O. N. Temkin and L. G. Bruk, "Palladium(II, I, 0) complexes in catalytic reactions of oxidative carbonylation," *Kinet. Catal.* **44**, 601–617 (2003).
- ³¹K. Novakovic, C. Grosjean, S. K. Scott, A. Whiting, M. J. Willis, and A. R. Wright, "Achieving pH and Qr oscillations in a palladium-catalysed phenylacetylene oxidative carbonylation reaction using an automated reactor system," *Chem. Phys. Lett.* **435**, 142–147 (2007).
- ³²J. Parker and K. Novakovic, "The effect of temperature on selectivity in the oscillatory mode of the phenylacetylene oxidative carbonylation reaction," *ChemPhysChem* **18**, 1981–1986 (2017).
- ³³K. Novakovic, L. Bruk, and O. Temkin, "History, versatility and future prospects of oscillatory carbonylation reactions of alkynes," *RSC Adv.* **11**, 24336–24344 (2021).
- ³⁴A. Isakova, B. J. Murdoch, and K. Novakovic, "From small molecules to polymeric catalysts in the oscillatory carbonylation reaction: Multiple effects of adding HI," *Phys. Chem. Chem. Phys.* **20**, 9281–9288 (2018).
- ³⁵A. Isakova and K. Novakovic, "Pulsatile release from a flat self-oscillating chitosan macrogel," *J. Mater. Chem. B* **6**, 5003–5010 (2018).
- ³⁶H. Sayama, *Introduction to the Modeling and Analysis of Complex Systems* (Open SUNY Textbooks, Geneseo, NY, 2015).
- ³⁷S. Mačeskić, Ž. Čupić, and L. Kolar-Anić, "Effect of diffusion on steady state stability of an oscillatory reaction model," *Chaos Soliton. Fract.* **174**, 113783 (2023).
- ³⁸B. L. Clarke, "Stability of complex reaction networks," in *Advances in Chemical Physics*, edited by I. Prigogine and S. Rice (John Wiley & Sons, Ltd, 1980), Vol. 43, pp. 1–215.
- ³⁹B. L. Clarke, "Stoichiometric network analysis," *Cell Biophys.* **12**, 237–253 (1988).
- ⁴⁰K. Novakovic, A. Mukherjee, M. Willis, A. Wright, and S. Scott, "The influence of reaction temperature on the oscillatory behaviour in the palladium-catalysed phenylacetylene oxidative carbonylation reaction," *Phys. Chem. Chem. Phys.* **11**, 9044–9049 (2009).
- ⁴¹S. P. Tonner, M. S. Wainwright, D. L. Trimm, and N. W. Cant, "Solubility of carbon monoxide in alcohols," *J. Chem. Eng. Data* **28**, 59–61 (1983).
- ⁴²K. Novakovic and J. Parker, "Catalyst initiation in the oscillatory carbonylation reaction," *Int. J. Chem. Eng.* **2011**, 1–11 (2011).
- ⁴³M. Quaranta, M. Murkovic, and I. Klimant, "A new method to measure oxygen solubility in organic solvents through optical oxygen sensing," *Analyst* **138**, 6243–6245 (2013).
- ⁴⁴Ž. Čupić, S. Mačeskić, K. Novakovic, S. Anić, and L. Kolar-Anić, "Stoichiometric network analysis of a reaction system with conservation constraints," *Chaos* **28**, 083114 (2018).
- ⁴⁵A. Logg, K.-A. Mardal, and G. Wells, *Automated Solution of Differential Equations by the Finite Element Method: The FEniCS Book* (Springer Science & Business Media, 2012), Vol. 84.
- ⁴⁶A. Jeffrey, *Applied Partial Differential Equations: An Introduction* (Academic Press, 2003).
- ⁴⁷Ž. Cupic, G. Schmitz, and L. Kolar-Anic, "Stoichiometric network analysis as mathematical method for examinations of instability region and oscillatory dynamics," *Sci. Publ. State Univ. Novi Pazar Ser. A* **8**, 43–64 (2016).
- ⁴⁸Ž. Čupić, V. Marković, A. Ivanović-Šašić, and L. Kolar-Anić, "Modeling of the complex nonlinear processes: Determination of the instability region by the stoichiometric network analysis," in *Mathematical Modelling*, edited by C. R. Brennan (Nova Science Publishers, Inc., New York, 2013), pp. 111–178.
- ⁴⁹G. Hadley, *Linear Programming* (Addison-Wesley Publishing Company, 1962).
- ⁵⁰C. H. Schilling, D. Letscher, and B. Ø. Palsson, "Theory for the systemic definition of metabolic pathways and their use in interpreting metabolic function from a pathway-oriented perspective," *J. Theor. Biol.* **203**, 229–248 (2000).
- ⁵¹B. L. Clarke, "Diffusion and chemical oscillations—Theory and calculations on a mechanism for the bromate-cerium-malonic acid system," *J. Chem. Phys.* **58**, 5605–5614 (1973).
- ⁵²B. L. Clarke, "Stoichiometric network analysis of the oxalate–persulfate–silver oscillator," *J. Chem. Phys.* **97**, 2459–2472 (1992).
- ⁵³B. L. Clarke and W. Jiang, "Method for deriving Hopf and saddle-node bifurcation hypersurfaces and application to a model of the Belousov–Zhabotinskii system," *J. Chem. Phys.* **99**, 4464–4478 (1993).
- ⁵⁴L. Orlando, "Sul problema di Hurwitz relativo alle parti reali delle radici di un'equazione algebrica (On the Hurwitz problem concerning the real parts of the roots of an algebraic equation)," *Math. Ann.* **71**, 233–245 (1911).
- ⁵⁵G. Schmitz, L. Z. Kolar-Anić, S. R. Anić, and Z. D. Čupić, "Stoichiometric network analysis and associated dimensionless kinetic equations. Application to a model of the Bray–Liebhafsky reaction," *J. Phys. Chem. A* **112**, 13452–13457 (2008).
- ⁵⁶V. M. Markovic, Z. Cupic, V. Vukojevic, and L. Kolar-Anic, "Predictive modeling of the hypothalamic-pituitary-adrenal (HPA) axis response to acute and chronic stress," *Endocr. J.* **58**, 889–904 (2011).

⁵⁷S. Macesic, Ž. Cupic, and L. Kolar-Anic, "Model of a nonlinear reaction system with autocatalysis and autoinhibition: Stability of dynamic states," *Hem. Ind.* **66**, 637–647 (2012).

⁵⁸S. Maćešić, Ž. Čupić, S. Anić, and L. Kolar-Anić, "Autocatalator as the source of instability in the complex non-linear neuroendocrine model," *Int. J. Non-Linear Mech.* **73**, 25–30 (2015).

⁵⁹B. Gabriele and G. Salerno, *Palladium(II) Iodide. Encyclopedia of Reagents for Organic Synthesis (EROS)* (John Wiley & Sons, Ltd, 2006).

⁶⁰A. Isakova, J. Parker, C. J. Nwosu, J. R. Howse, and K. Novakovic, "Broadening the scope of Pd-catalyzed oscillatory carbonylation reactions: Solvent, substrate, catalyst," *React. Kinet., Mech. Catal.* **127**, 161–174 (2019).